HORIZON EUROPE PROGRAMME
HORIZON-CL4-2023-DIGITAL-EMERGING-01-33

GA No. 101135196

Developing New 2D Materials and Heterostructures for Printed Digital Devices

2D-PRINTABLE - Deliverable report

D4.4 – Characterization of Networks and Heterostructures

Funded by
the European Union

Deliverable No.	D4.4	
Related WP	WP4	
Deliverable Title	Characterization of Networks and Heterostructures	
Deliverable Date	31/09/26	
Deliverable Type	REPORT	
Dissemination level	Public (PU)	
Author(s)	J Coleman (TCD)	2026-08-18
Checked by	Claudia Backes (UKa)	2026-08-19
Reviewed by	Claudia Backes (UKa) Zdenek Sofer (VSCHT)	2026-08-19 2026-08-19
Approved by	Jonathan Coleman (TCD) - Project Coordinator	2026-08-24
Status	Final	2026-08-24

Document History

Version	Date	Editing done by	Remarks
V1.0	18/08/26	J Coleman	Draft
V1.1	19/08/26	C Backes	reviewed
V2.0	19/08/26	Z Sofer	reviewed
FINAL	24/08/26	J Coleman	Final

Project Scientific Abstract

The 2D-PRINTABLE project aims to integrate sustainable large-scale liquid exfoliation techniques with theoretical modelling to efficiently produce a wide range of new 2D materials (2DMs), including conducting, semiconducting, and insulating nanosheets. The focus includes developing the printing and liquid phase deposition methods required to fabricate networks and multicomponent heterostructures, featuring layer-by-layer assembly of nanometer-thick 2DMs into ordered multilayers. The goal is to optimize these printed networks and heterostructures for digital systems, unlocking new properties and functionalities. The project also seeks to demonstrate various printed digital devices, including proof-of-principle, first-time demonstration of all-printed, all-nanosheet,

heterostack light-emitting diodes (LEDs). In conclusion, 2D-PRINTABLE will prove 2D materials to be an indispensable material class in the field of printed electronics, capable of producing far-beyond-state-of-the-art devices that can act as a platform for the next generation of printed digital applications.

Summary

This deliverable reports the characterization of solution-processed two-dimensional (2D) nanosheet networks and heterostructures developed within WP4 of 2D-PRINTABLE. The work combines established spectroscopic and microscopic methods with advanced three-dimensional imaging and impedance-based analysis. Particular emphasis is placed on methods that quantify nanosheet dimensions and quality, network thickness and uniformity, nanosheet orientation, porosity, tortuosity, interface quality and, where useful, the electrical consequences of network morphology. The characterization strategy therefore spans length scales from individual nanosheets to complete multilayer device stacks.

At nanosheet level, UV-vis/extinction spectroscopy, Raman spectroscopy, photoluminescence (PL), transmission electron microscopy (TEM) and atomic force microscopy (AFM) were used to establish composition, structural quality, lateral dimensions, thickness and aspect ratio. These measurements show, for example, the very different dimensions and aspect ratios obtained by liquid-phase exfoliation (LPE) and electrochemical exfoliation (EE), and provide the statistical inputs required to interpret the morphology of deposited networks. At network level spectroscopy was used for basic characterisation while SEM, cross-sectional SEM and FIB-SEM nanotomography were used to visualize internal structure and quantify parameters including porosity, tortuosity, roughness and nanosheet alignment. For example, high-aspect-ratio nanosheets form markedly denser and more aligned networks than low-aspect-ratio LPE material. Mechanical compression of porous WS2 networks further demonstrates how the same characterization toolkit can quantify processing-induced changes in morphology.

A complementary set of spatially averaged methods was developed for rapid characterization of large-area films. Optical transmission scanning provides local thickness maps and a thickness-dispersity index, while polarized Raman spectroscopy provides the Hermans orientation parameter. Across MoS2 networks prepared by different deposition routes, these independent measures show the same ordering of assembly quality. Impedance spectroscopy provides an additional network-homogeneity parameter, n, which tracks both thickness uniformity and orientational order and, importantly, correlates with the microscopic transport ratio RJ/RNS. Thus, impedance is used here not simply as an electrical measurement, but as a morphology-sensitive characterization method that reports on the distribution of junction properties within the network.

Finally, the characterization approach was extended to solution-processed multilayers and heterostructures. AFM and optical transmission scanning verified compact, highly uniform MoS2 layers, while UPS/LEIPS established energy levels needed for heterostructure design. Cross-sectional SEM verified smooth, pinhole-free interfaces in complete multilayer stacks, and PL measurements confirmed retention of emissive properties following nanocomposite and heterostructure fabrication. Together, these results demonstrate a coherent characterization framework for linking nanosheet quality, network assembly and heterostructure integrity to the properties required for printed digital devices.

Contents

List of Figures

Abbreviations & Definitions

AFM: atomic force microscopy

EE: electrochemical exfoliation

FIB-SEM: focused-ion-beam scanning electron microscopy

I: thickness dispersity index

KPFM: Kelvin probe force microscopy

LEIPS: low-energy inverse photoemission spectroscopy

LLID: liquid-liquid interfacial deposition

LPE: liquid-phase exfoliation

PL: photoluminescence

RJ / RNS: inter-nanosheet junction resistance / nanosheet resistance

S: Hermans orientation parameter

SEM / TEM: scanning / transmission electron microscopy

UPS: ultraviolet photoelectron spectroscopy

WLI: white-light interferometry

1 Introduction

WP4 addresses the characterization of exfoliated and functionalized nanosheets, printed nanosheet networks and heterostructures using complementary spectroscopic and microscopic methods. The work is designed both to provide reliable routine characterization and to develop quantitative descriptors that can be linked to network assembly and, ultimately, device performance. In the Description of Action, the planned methods include Raman and IR spectroscopy, optical extinction/absorption/PL, AFM, TEM, SEM, Raman mapping and FIB-SEM nanotomography, with advanced methods used to assess interfaces, band alignment and intrinsic transport where appropriate.

D4.4 consolidates results obtained on representative graphene, WS_2 and MoS_2 nanosheet systems. The emphasis is on characterization of deposited networks and heterostructures rather than on device optimization itself. Electrical methods are included only where they provide complementary structural information or allow the consequences of morphology to be quantified. This is particularly important for impedance spectroscopy, which can distinguish nanosheet and junction contributions and, as shown below, can also provide a quantitative measure of network heterogeneity.

The results demonstrate that the planned WP4 objectives have been met at multiple levels: standard spectroscopy and microscopy establish nanosheet quality and dimensions; SEM, AFM and optical mapping quantify network uniformity and surface morphology; FIB-SEM provides quantitative 3D structural descriptors; polarized Raman provides a non-contact measure of orientational order; and multilayer heterostructures can be assessed through cross-sectional imaging, optical spectroscopy and experimental energy-level measurements. These methods together provide the characterization basis required to optimize printing/deposition and to support subsequent electrical and device work in WP5 and WP6.

2 Methods and characterization framework

Standard nanosheet and optical characterization

Firstly, the individual nanosheets making up the networks were characterized by TEM and AFM to establish morphology, lateral dimensions and thickness distributions. Statistical AFM was particularly important because nanosheet length and thickness determine aspect ratio and provide quantitative inputs for interpreting network assembly. UV-vis/extinction spectra were used as rapid optical fingerprints of dispersed nanosheets and size-selected fractions. Raman spectroscopy verified characteristic vibrational modes and provided information on defects, strain and, in polarized measurements, orientation. For semiconducting MoS_2, absorption and PL measurements, including calibrated PL quantum yield, were also used to assess the optical quality and doping-dependent emissive response of deposited nanosheets.

Network morphology, thickness and 3D structure

Surface and cross-sectional SEM were used to assess packing, alignment, porosity and the integrity of interfaces. AFM was used both for nanosheet statistics and for film roughness. Large-area thickness uniformity was assessed using optical transmission scanning: local transmission was converted to optical extinction, which is proportional to local film thickness, allowing thickness distributions and a normalized thickness-dispersity index I to be extracted with spatial resolution of approximately 10 micrometres. For selected networks, FIB-SEM nanotomography was used to reconstruct the internal nanosheet and pore volumes in three dimensions and to quantify porosity, tortuosity, roughness and orientation.

Polarized Raman and network orientational order

Polarized Raman spectroscopy was applied to deposited MoS_2 networks to quantify nanosheet orientation over areas much larger than those accessible to local microscopy. The angular dependence of the Raman intensity was fitted to extract the Hermans orientation parameter S, where S approaches unity for highly ordered in-plane nanosheet alignment. This provides a complementary morphology metric to the thickness-dispersity index obtained from transmission scanning.

Impedance spectroscopy as a complementary characterization tool

Impedance spectra were analysed using equivalent-circuit and network models in which the fundamental unit is a nanosheet resistance RNS in series with a junction element containing RJ and junction capacitance CJ. This allows average nanosheet and junction contributions to be separated. In structurally heterogeneous networks, the distribution of junction time constants broadens the impedance response; the corresponding ideality/homogeneity parameter n therefore contains information on the width of the microscopic junction-property distribution. As discussed in Section 3.4, this makes impedance spectroscopy a useful morphology-sensitive probe rather than only an electrical test.

Characterization of multilayers and heterostructures

For solution-processed multilayers and heterostructures, characterization focused on whether each deposition step produced continuous, uniform films without damaging underlying layers. Optical transmission scanning and AFM were used to quantify thickness and roughness; cross-sectional SEM verified the stacked architecture and interface continuity. UPS and LEIPS were used to determine valence- and conduction-band energetics of MoS_2 films, while absorption and PL measurements assessed whether optical functionality was retained following nanocomposite formation and subsequent layer deposition.

3 Results & Discussion

3.1 Nanosheet-level characterization

The network studies were underpinned by routine nanosheet characterization. For graphene prepared by LPE and EE, UV-vis extinction spectra showed the expected graphene response, while Raman spectra distinguished the different defect contents of the two materials. TEM confirmed well-exfoliated 2D objects and AFM established strongly different size distributions: the EE material had a mean thickness of approximately 1.08 nm and mean length of approximately 1.88 micrometres, compared with approximately 7.0 nm and 0.66 micrometres for LPE graphene. The corresponding mean aspect ratios were approximately 2083 and 108. These statistics are central to interpreting why the two materials assemble differently after deposition.

Comparable multi-technique characterization was applied to WS_2 and MoS_2. Size-selected LPE WS_2 fractions were monitored by extinction spectroscopy, Raman spectroscopy and AFM; the A_{1g} and E_{2g} Raman modes confirmed 2H-WS_2, while AFM length/thickness statistics were consistent with liquid-cascade-centrifugation scaling. In the EE MoS_2 systems, TEM showed large, thin nanosheets with clean edges and AFM established few-layer thickness distributions. In the LED-oriented MoS_2 work, AFM, absorption, PL and calibrated PLQY measurements provided a complementary assessment of monolayer dimensions, colloidal environment and optical quality. Together, these measurements demonstrate that network characterization begins with quantitative knowledge of the nanosheet building blocks rather than treating the deposited film as a black box.

3.2 Basic characterization of deposited nanosheet networks

A first level of network characterization uses rapid, widely available optical and microscopic methods to establish material identity, film thickness and basic morphology. Figure 1A shows UV-visible optical extinction spectra of WS_2 nanosheet networks prepared by liquid-liquid interfacial deposition (LLID) using one to five sequential deposition cycles. The spectral features provide a characteristic fingerprint of the deposited nanosheets, while the overall extinction increases systematically with the number of deposited layers. After calibration, this type of measurement can therefore also provide a convenient estimate of network thickness or deposited material quantity.

Raman spectroscopy provides complementary information on the composition and state of deposited nanosheets. Representative spectra from LLID films of MoS_2, InSe and $MoWSe_2$ are shown in Figure 1B. The characteristic vibrational modes identify the material present in the network and, depending on the system, changes in peak position, width or intensity can additionally provide information on factors such as strain, doping, defects or inter-nanosheet interactions even though this is often not achievable in solution processed networks opposed to grown films..

Direct imaging is required to visualize how nanosheets assemble into a network. Figure 1C and D compare SEM images of MoS_2 films made using different nanosheet types and deposition routes. The spray-coated network formed from liquid-phase-exfoliated, relatively low-aspect-ratio nanosheets is visibly disordered, whereas the LLID network formed from electrochemically exfoliated, high-aspect-ratio nanosheets is much more compact and tiled. Such images provide an immediate qualitative assessment of nanosheet alignment, packing and junction geometry before more quantitative analysis is undertaken.

A further basic requirement is reliable measurement of the average network thickness. White-light interferometry (WLI) provides a simple and robust approach for this purpose. In the example in Figure 1E, a narrow region of a MoS_2 nanosheet network was manually removed to expose the underlying substrate. The resulting trench provides a height reference, allowing the local film thickness to be mapped over a relatively large area. Repeated measurements across the map yield both an average network thickness and its associated spatial variation.

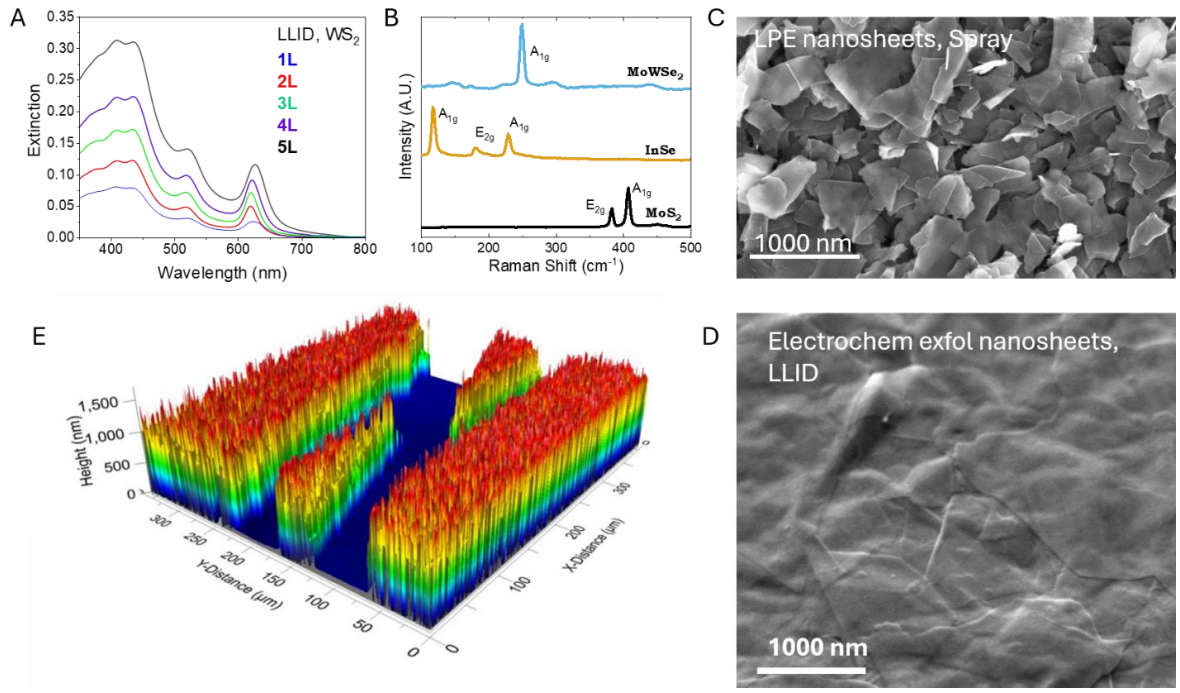

Figure 1. Basic characterization of nanosheet networks. (A) UV-visible optical extinction spectra of WS_2 nanosheet networks prepared by liquid-liquid interfacial deposition (LLID) for one to five deposited layers. (B) Representative Raman spectra of LLID films prepared from MoS_2, InSe and $MoWSe_2$ nanosheets. (C,D) SEM images of MoS_2 networks comprising liquid-phase-exfoliated (LPE), relatively low-aspect-ratio nanosheets deposited by spray coating (C) and electrochemically exfoliated, high-aspect-ratio nanosheets deposited by LLID (D). (E) White-light interferometry map of a MoS_2 nanosheet network after manual scraping to expose the substrate; the resulting trench provides a height reference for film-thickness measurement.

3.3 Three-dimensional network morphology

A direct demonstration of the impact of nanosheet geometry on network structure is obtained by comparing spray-coated LPE and EE graphene. Cross-sectional SEM shows the LPE film to be porous and poorly aligned, whereas the EE network appears much denser and more planar. FIB-SEM nanotomography converts this qualitative difference into quantitative 3D descriptors. The LPE network has a porosity of approximately 43% and an in-plane tortuosity factor of approximately 1.38; the EE network has a porosity of only approximately 2% and a tortuosity of approximately 1.05. The much lower roughness and stronger in-plane alignment of the EE film are consistent with high-aspect-ratio nanosheets conforming to neighbouring sheets and forming large-area contacts.

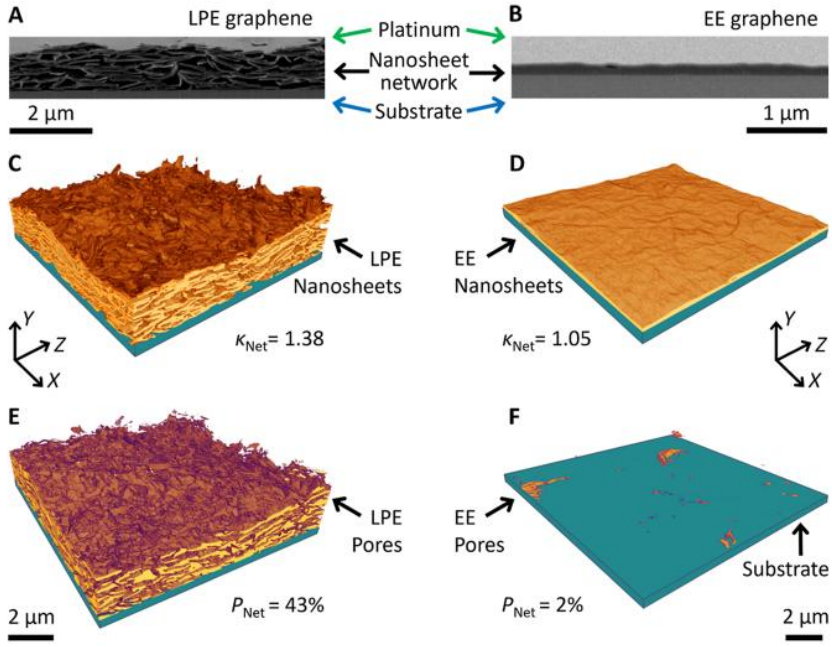

Figure 2. Microscopic network characterization. Cross-sectional SEM and FIB-SEM nanotomography compare spray-coated graphene networks made from low-aspect-ratio LPE nanosheets and high-aspect-ratio EE nanosheets. Cross sectional images are shown in A and B. 3D images are shown for networks of nanosheets (C &E) as well as inter-nanosheet pores (D &F). The LPE network is porous and disordered, whereas the EE network is dense, highly aligned and close to monolithic. Reproduced from 2D-PRINTABLE project results.

The value of this approach is that parameters such as porosity, tortuosity and orientation can be measured directly and then compared across deposition methods, materials and post-treatments. These are also the parameters expected to control interface quality in heterostacks: a rough, porous upper surface will produce a very different interface to a dense, smooth and well-aligned network.

3.4 Impedance spectroscopy as a network characterization method

Impedance spectroscopy was developed as a method for separating nanosheet and junction contributions within deposited semiconducting networks. For EE MoS_2, the measured complex network resistivity was converted to the impedance of an average nanosheet-junction pair. Fitting the frequency response gave typical values RJ = 2.9 MOhm, RNS = 0.67 MOhm and CJ = 8.4 fF, corresponding to RJ/RNS approximately 4.4. The method was cross-checked against independent measurements: single-nanosheet mobility gave a similar RJ/RNS estimate, while in-operando KPFM directly visualized gradual potential drops within nanosheets and sharp drops at inter-sheet junctions.

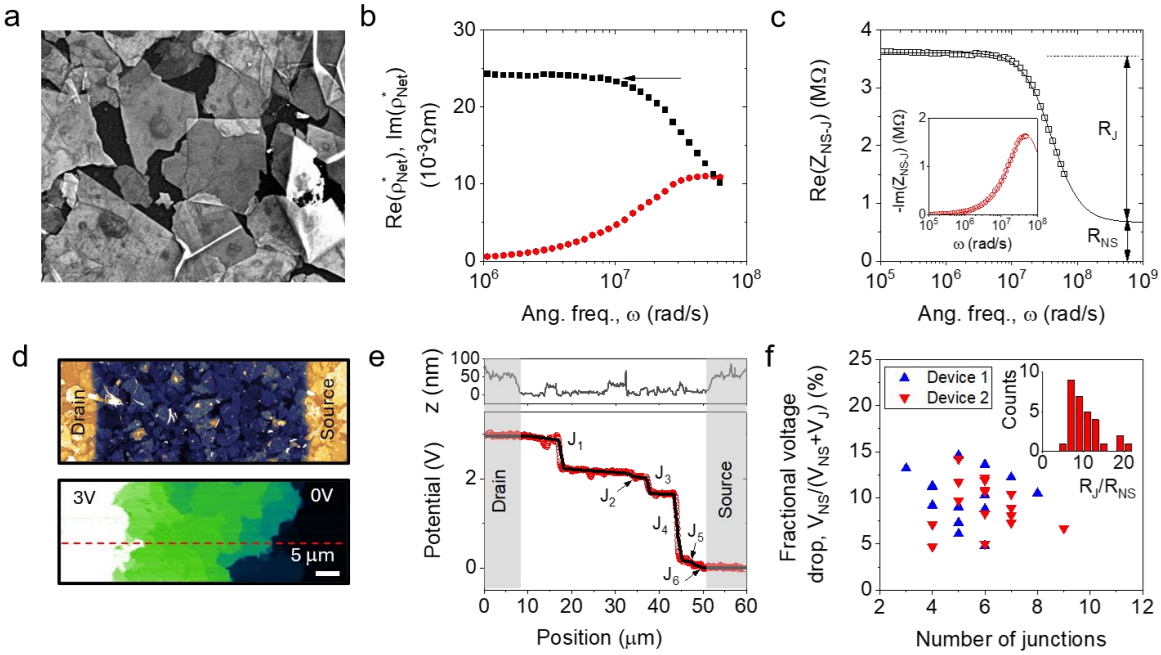

Figure 3. Identification of nanosheet and junction resistances in EE MoS2 networks. The figure combines SEM (A), network impedance spectra and equivalent-circuit analysis (B-C) with AFM/KPFM validation (D-F). The frequency-dependent response separates RNS from RJ and CJ, while KPFM independently visualizes voltage drops at individual junctions. Reproduced from 2D-PRINTABLE project results.

Although this is an electrical measurement, its relevance to D4.4 is broader: the shape and broadening of the impedance response depend on the distribution of junction properties throughout the film. This observation motivated the use of impedance-derived parameters as descriptors of network homogeneity, which was then tested directly against independent morphological measurements.

3.5 Network homogeneity from scanner, polarized Raman and impedance

A particularly useful characterization framework was developed using high-aspect-ratio EE MoS_2 deposited by four different routes: liquid-liquid interfacial deposition (LLID), dip coating, spray coating and spin coating. SEM showed clear differences in assembly. Transmission scanning provided pixel-by-pixel extinction maps and thickness distributions; from these, the thickness-dispersity index I was extracted. Polarized Raman measurements independently quantified orientational order through the Hermans parameter S.

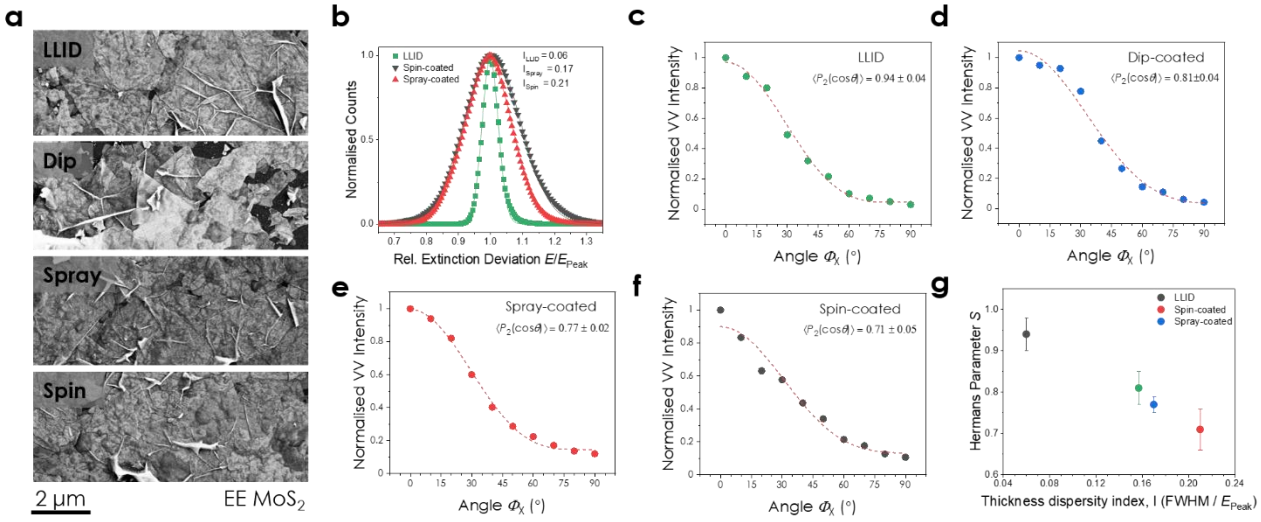

Figure 4. Morphological characterization of EE MoS_2 networks prepared by LLID, dip coating, spray coating and spin coating. SEM images (A) are combined with optical-transmission-derived thickness distributions (B) and polarized Raman measurements (C-F). The Hermans orientation parameter S correlates with the thickness-dispersity index I, demonstrating consistency between independent measures of network assembly quality (G). Reproduced from 2D-PRINTABLE project results.

The key result is the consistency of the different characterization methods. LLID produced the most ordered films, with S approximately 0.94 and I approximately 0.06; spin coating gave the least ordered films, with S approximately 0.71 and I approximately 0.21; dip- and spray-coated films were intermediate. Thus a film that is more uniform in thickness is also more ordered in nanosheet orientation. The agreement is important because scanner measurements probe large-area thickness variations whereas polarized Raman probes nanosheet orientational order through an entirely different physical mechanism.

Impedance spectroscopy showed the same deposition-dependent hierarchy. The impedance-derived homogeneity parameter n was highest for LLID (approximately 0.92) and lowest for spin coating (approximately 0.81), with dip and spray again intermediate. Strong correlations were found between n and both S and I: n increases with orientational order and decreases as thickness dispersity increases. This demonstrates that the impedance response contains quantitative information about morphology and assembly quality. The parameter n should not be interpreted as reporting orientation alone; instead, it reflects the distribution of microscopic junction properties and therefore responds to several structural variables, including alignment, overlap geometry, packing density and inter-sheet spacing.

Most importantly, n also correlates with the transport ratio RJ/RNS. Better assembled, more homogeneous networks have narrower junction-property distributions and lower junction limitation, whereas more disordered networks show reduced n and larger RJ/RNS. The combined data therefore establish a continuous characterization chain: deposition method controls thickness uniformity and nanosheet orientation; these features determine junction uniformity; impedance quantifies that junction heterogeneity through n; and n predicts the extent to which transport is junction limited. This is a useful outcome for rapid network screening because it allows a single impedance measurement to provide both transport information and a proxy for network morphological quality.

3.6 Processing-induced changes in network morphology

The same characterization concepts were applied to a range of different networks. For example, we studied LPE WS_2 networks subjected to uniaxial compression. Extinction spectroscopy and AFM first established the dimensions of size-selected nanosheets, while Raman spectroscopy verified the WS_2 structure and was subsequently used as a strain-sensitive probe. After compression, the A_{1g} Raman mode shifted to higher frequency, with a size-dependent response that indicates more efficient inter-nanosheet stress transfer for larger nanosheets over an intermediate size range.

SEM and FIB-SEM nanotomography show that compression dramatically densifies the network. In a representative WS_2 film, porosity fell from approximately 39% to 5% and tortuosity from approximately 1.43 to 1.07. Across size-selected networks, roughness, porosity and tortuosity all decreased after compression, with the largest changes generally found for networks of larger nanosheets. This demonstrates how 3D characterization can quantify processing-induced morphology changes even when no change in material chemistry is involved. The reduced surface roughness is also directly relevant to heterostructures, because smoother networks provide higher-quality interfaces for subsequent layers.

Electrical measurements were used only to test the consequences of these structural changes. Compression increased conductivity and reduced junction resistance by roughly an order of magnitude, but impedance and temperature-dependent data showed that the junctions remained effectively point-like. Thus, densification improves contact quality without converting low-aspect-ratio LPE networks into the conformal large-area junction morphology characteristic of high-aspect-ratio EE networks. This distinction reinforces the importance of combining imaging, Raman and impedance rather than inferring morphology from conductivity alone.

3.7 Characterization of multilayers and heterostructures

Characterization was extended from single networks to solution-processed multilayer heterostructures relevant to printed devices such as PV cells and LEDs. AFM of spin-coated MoS_2 films showed compact nanosheet layers, while optical transmission scanning provided a rapid test of thickness uniformity and solvent compatibility. For films produced with one to four deposition cycles, the thickness distributions were near-Gaussian with FWHM values below 10% of the mean thickness. Mean thickness increased linearly with deposition number by approximately 22 nm per coating cycle, indicating controlled multilayer build-up and negligible loss of previously deposited material after the adopted thermal treatment.

The optical transmission method was also used to quantify whether candidate solvents damaged existing MoS_2 layers. DMF produced a substantial thickness reduction in unprotected films, whereas water, chlorobenzene and hexane caused minimal change. These measurements directly informed the orthogonal-solvent strategy required to fabricate multilayer solution-processed heterostructures without dissolving or redistributing underlying layers.

Spectroscopic characterization was used to establish functionality as well as morphology. Absorption and PL measurements characterized the emissive response of the MoS_2 nanosheets and highlighted the sensitivity of PL to the colloidal/doping environment. Formation of MoS_2:PVK nanocomposites and subsequent ZnO deposition did not significantly degrade the PL response, showing that the heterostructure fabrication sequence retained the optical functionality of the emissive nanosheets. AFM measured a very smooth MoS_2:PVK surface, with average roughness of approximately 0.8 nm for a film around 27 nm thick, supporting formation of a high-quality interface with the overlying ZnO/PEIE layer.

UPS and LEIPS provided an advanced, non-microscopic characterization of the electronic structure of the deposited MoS_2 film. The measured ionization energy and electron affinity were approximately -5.62 eV and -3.80 eV, respectively, corresponding to an experimental gap of approximately 1.82 eV and allowing the energy-level alignment of the full multilayer stack to be designed from measured rather than assumed values. Finally, cross-sectional SEM verified successful formation of the complete heterostructure, with the individual layers stacked smoothly and without obvious pinholes. These measurements demonstrate that the WP4 characterization framework can follow a material from dispersed nanosheets through uniform networks to a complete functional heterostructure.

3.8 Integrated structure-property picture

Taken together, the five studies establish a consistent multiscale picture. Nanosheet dimensions and aspect ratio are first established by AFM/TEM and optical/Raman spectroscopy. These building-block properties influence network packing, which can be observed by SEM and quantified in three dimensions by FIB-SEM. Large-area scanner measurements and polarized Raman then provide statistically robust descriptors of thickness uniformity and orientation. Impedance spectroscopy adds a complementary parameter n that reports the distribution of microscopic junction properties and links directly to RJ/RNS. Finally, multilayer characterization verifies whether the resulting network surfaces, interfaces and band alignments are suitable for heterostructure assembly.

The central outcome is therefore methodological as well as scientific: no single characterization technique is sufficient. Local imaging is required to visualize structure, statistical optical and Raman methods are required to assess large-area uniformity and order, and impedance provides a route to connect that morphology to the junction population that governs charge transport. The agreement between these independent measurements gives confidence that the derived structural descriptors are meaningful and transferable to future 2D-PRINTABLE materials and heterostructures.

3.9 Contribution to project (linked) Objectives

D4.4 contributes directly to WP4 Objective O4.2, establishing basic and advanced characterization of nanosheet networks and heterostructures to assess morphology and nanosheet coupling, and to O4.3 through the development/application of new methodologies for network characterization. It also supports the project-level objective of characterizing solution-deposited networks and heterostructures using 3D imaging and direct junction characterization. The demonstrated combination of FIB-SEM nanotomography, optical thickness mapping, polarized Raman, impedance-derived homogeneity analysis and heterostructure band/interface characterization provides the quantitative feedback needed for deposition optimization in WP3 and device integration in WP6.

3.10 Contribution to major project exploitable result

The principal exploitable result is a transferable characterization workflow for printed nanosheet networks and heterostructures. The workflow combines widely accessible methods (UV-vis/extinction, Raman, AFM, TEM and SEM) with advanced methods (FIB-SEM, polarized Raman, impedance analysis, UPS/LEIPS and KPFM) and identifies quantitative descriptors that can be used to compare materials and deposition routes. Particularly valuable is the ability to connect fast, large-area descriptors of film quality to microscopic junction behavior: scanner-derived thickness dispersity, Raman-derived orientational order and impedance-derived n all track network assembly, while n predicts RJ/RNS. This provides a practical route for screening and optimizing printed networks before full device fabrication.

4 Conclusion and Recommendation

D4.4 demonstrates comprehensive characterization of 2D-PRINTABLE nanosheet networks and heterostructures using complementary spectroscopic, microscopic and electrical methods. Routine nanosheet characterization by extinction spectroscopy, Raman, TEM and AFM establishes the dimensions and quality of the building blocks. SEM and FIB-SEM reveal how nanosheet aspect ratio and processing determine network packing and provide quantitative measures of porosity, tortuosity, roughness and alignment. Optical transmission scanning and polarized Raman provide scalable measures of thickness uniformity and orientation, while impedance spectroscopy supplies an independent network-homogeneity parameter that correlates with these morphological descriptors and with RJ/RNS. Multilayer and heterostructure work shows that AFM, scanner measurements, PL, UPS/LEIPS and cross-sectional SEM can verify thickness control, optical functionality, band alignment and interface integrity in complete solution-processed stacks.

The main recommendation is to continue using characterization as an integrated workflow rather than selecting techniques independently. For new networks, AFM/TEM and optical/Raman measurements should establish nanosheet statistics before deposition; scanner and polarized Raman measurements can then rapidly rank large-area network uniformity and orientation; FIB-SEM should be reserved for representative samples where full 3D structural quantification is required; and impedance-derived n should be used alongside these methods where junction uniformity and transport limitation are important. For multilayer heterostructures, optical thickness mapping, AFM roughness, cross-sectional SEM and experimental band-level measurements should be combined to verify that each deposition step preserves the underlying structure and produces the intended interface.

5 Risks and interconnections

5.1 Risks/problems encountered

No significant risks or problems were encountered that prevented the objectives of this deliverable from being achieved. Some advanced methods are inherently sample-dependent: FIB-SEM is most informative for porous or compositionally distinguishable networks, while ultrahigh-vacuum electronic-structure measurements require sufficiently clean and robust deposited films. These limitations were managed by using complementary techniques and by applying each method where it provides the most reliable information.

5.2 Interconnections with other deliverables

The characterization results are closely interconnected with WP1-WP3, where nanosheets, inks, networks and heterostructures are produced, in particular D3.3 “Printed heterostructure fabrication” and D4.1 “Characterization of nanosheets, networks and heterostacks built from initially available 2D materials”, and with WP5-WP6, where their electrical properties and device performance are evaluated, in particular D5.1 “Electrical characterization of LPE derived novel materials” and D5.3 “Electrical characterization of films and vertical heterostructures” and all deliverables connected to WP6. Nanosheet-size and quality metrics provide feedback to exfoliation/size-selection; morphology and homogeneity metrics provide feedback to printing/deposition; and junction/interface characterization informs optimization of transport and charge injection. The multilayer characterization described here directly supports the fabrication of printed heterostructures and all-nanosheet device stacks.

6 Deviations from Annex 1

No deviations from Annex 1 are reported for the activities covered by this deliverable.

7 References

Not applicable. The deliverable reports 2D-PRINTABLE project results without a separate bibliography.

Acknowledgement

The author(s) would like to thank the partners in the project for their valuable comments on previous drafts and for performing the review.

Project partners:

#	Partner short name	Partner Full Name
1	TCD	TCD THE PROVOST, FELLOWS, FOUNDATION SCHOLARS & THE OTHER MEMBERS OF BOARD, OF THE COLLEGE OF THE HOLY & UNDIVIDED TRINITY OF QUEEN ELIZABETH NEAR DUBLIN
2	UNISTRA	UNIVERSITE DE STRASBOURG
3	UKa	UNIVERSITAET KASSEL
4	BED	BEDIMENSIONAL SPA
5	TUD	TECHNISCHE UNIVERSITAET DRESDEN
6	VSCHT	VYSOKA SKOLA CHEMICKO-TECHNOLOGICKA V PRAZE
7	UNR	UNIRESEARCH BV
8	UniBw M	UNIVERSITAET DER BUNDESWEHR MUENCHEN
9	EPFL	ECOLE POLYTECHNIQUE FEDERALE DE LAUSANNE

Disclaimer/ Acknowledgment

This project has received funding from the European Union's Horizon Europe research and innovation programme under grant agreement No 101135196. Views and opinions expressed are however those of the author(s) only and do not necessarily reflect those of the European Union. Neither the European Union nor the granting authority can be held responsible for them.